Check for updates

Vertically stacked SnSe homojunctions and negative capacitance for fast low-power tunneling transistors†

Hong Li, [ID] *[a] Jiakun Liang,[a] Peipei Xu,[a] Jing Luo[b] and Fengbin Liu[a]

The two-dimensional (2D) vertical van der Waals (vdW) stacked homojunction is an advantageous configuration for fast low-power tunneling field effect transistors (TFETs). We simulate the device performance of the sub-10 nm vertical SnSe homojunction TFETs with *ab initio* quantum transport calculations. The vertically stacked device configuration has an effect of decreasing leakage current when compared with its planar counterpart due to the interrupted carrier transport path by the broken connection. A subthreshold swing over four decades ($SS_{ave\_4\ dec}$) of 44.2–45.8 mV dec^{-1} and a drain current at SS = 60 mV dec^{-1} (I_{60}) of 5–7 μA μm^{-1} are obtained for the optimal vertical SnSe homojunction TFET with L_g = 10 nm at a supply voltage of 0.5–0.74 V. In terms of the device's main figures of merit (*i.e.*, on-state current, intrinsic delay time, and power delay product), the vertical SnSe TFETs and NCTFETs outperform the 2022 and 2028 targets of the International Technology Roadmap for Semiconductors requirements for low-power application (2013 version), respectively.

1 Introduction

A tunneling field effect transistor (TFET) is a competitive post-CMOS low-power (LP) switch for future nano-electronics because avoiding thermionic carrier injection produces sub-60 mV dec^{-1} subthreshold swings (SS).[1–4] The main challenge in adopting TFETs for real application is the low on-state currents (I_{on}) despite the sharp minimum SS. The use of two-dimensional (2D) (instead of 3D) semiconductors (*e.g.*, black phosphorene (BP), bismuthine, GeSe, and SnSe) as channel materials can effectively improve I_{on} to enable TFETs even for high-performance (HP) applications with a single channel material and a simple planar p–i–n device configuration.[5–8] However, unacceptably high leakage currents (I_{leak}) for LP applications are also found at the ultrashort sub-10 nm size. The planar ML SnSe TFET is one example.[5] To reduce I_{leak}, structural modifications that can produce an additional tunneling barrier are appreciated. The vertically stacked configuration, *i.e.*, to overlap a top and a bottom layer vertically

in the channel region, is one suggested structural modification to lower I_{leak}.[9]

As the first discovered 2D material with anisotropic charge transport characters, monolayer (ML) and few-layers BP are expected as the potential channel materials for next-generation nano-electronics like transistors and have been extensively investigated in labs.[10–13] However, the excellent semiconducting properties of 2D BP would rapidly lose upon exposure to ambient conditions, which would somehow ruin the original outstanding device performances. Though air-stable 2D BP devices are realized by protective layers[14–16] and ambient thermal treatment,[17] the increased cost would undoubtedly hamper future large-scaled applications. Therefore, exploring new 2D channels with both excellent electronic properties and high stability is crucial for the manufacturing process of future nano-electronics. As one of BP analogs, ML and few-layers SnSe have been synthesized in labs in recent years.[18–20] Similar to ML BP, ML SnSe is low-toxic and possesses excellent electronic properties like anisotropic electronic, moderate near direct bandgap, and high carrier mobility.[21–23] Moreover, 2D SnSe has good ambient stability[22,24] and economic earth-abundance elements, which are another two advantages for practical future nano-electronics. Considering the high current of the planar ML SnSe TFET and the above benefits, it's meaningful to find out whether the vertically stacked SnSe homojunction, which is much less studied than the planar configuration, could enable the SnSe TFET as fast LP device in regard to the International Technology Roadmap for Semiconductors (ITRS) requirements (2013 version). Besides, to find out whether the

aCollege of Mechanical and Material Engineering, North China University of Technology, Beijing 100144, P. R. China. E-mail: lihong@ncut.edu.cn

bBeijing Research Institute of Automation for Machinery Industry, Beijing 100120, P. R. China

† Electronic supplementary information (ESI) available: The optimized lattices and band gaps with the PBE, Grimme DFT-D2, and Grimme DFT-D3 functionals; I_{on} and I_{leak} of the vertical SnSe TFETs with stacked sites; I_{on} and I_{leak} of the vertical SnSe TFETs with N_s/N_d; SS_{min}, $SS_{ave\_4\ dec}$, and I_{60} of the optimal vertical SnSe TFETs; transfer characteristics of the vertical SnSe TFETs with stacked sites and N_s/N_d. See DOI: 10.1039/d0ra03279d

negative capacitance effect could improve the device performances evidently is also a meaningful issue.

In this paper, we investigate the device performances of the sub-10 nm vertical SnSe homojunction TFETs with *ab initio* quantum transport calculations. A sub-thermionic SS over four decades ($SS_{ave\_4\ dec}$) of 44.2–45.8 mV dec^{-1} and a drain current at SS = 60 mV dec^{-1} (I_{60}) of 5–7 μA μm^{-1} are obtained for the 10 nm optimal vertical SnSe homojunction TFETs. The sub-thermionic $SS_{ave\_4\ dec}$ and high I_{60} indicate a fast low-power device. The device performances (*i.e.*, on-state current, intrinsic delay time, and power delay product) of this sub-10 nm vertical SnSe TFETs and NCTFETs surpass the 2022 and 2028 targets of the ITRS LP device (2013 version), respectively.

2 Models and methods

We first optimized the ML SnSe and bilayer (BL) SnSe with the density functional theory (DFT) using QuantumATK.[25,26] We use a norm-conserving pseudopotential of 'SG15' with 'Medium' basis set, a cutoff energy of 100 Ha, an exchange–correlation functional in the form of generalized gradient approximation of Perdew–Burke–Ernzerh (GGA-PBE)[27] with Grimme DFT-D2 correction,[28] and a Monkhorst–Pack mesh[29] of 31 × 31 × 1 k-points, and an electron temperature of 300 K. To judge the DFT-D2 functional, we compare the optimized lattice and band gap of bulk, bilayer, and ML SnSe obtained with three functionals, *i.e.*, PBE, Grimme DFT-D2, and Grimme DFT-D3, in Table S1.† The DFT-D2 functional gives the best lattice cells among the three checked functionals to reproduce the former theoretical and experimental results.[30]

The double-gated (DG) device model of the vertical SnSe homojunction TFET is presented in Fig. 1(a), where two optimized ML SnSe are stacked vertically with van der Waals interaction and the distance of the top and bottom layer of the vertical SnSe TFET is taken from optimized BL SnSe. Only the zigzag transport direction with lighter effective mass is studied due to the higher on-state current (I_{on}), as shown in a previous work.[5] The stacked overlap region is around 1 nm, and the stacked sites (*i.e.*, the position of the 1 nm overlap region of the top and bottom layer of SnSe) at the left, central, and right and the source/drain doping concentrations (N_s/N_d) are taken into consideration to optimize I_{on} of the vertical SnSe TFET with a physical gate length (L_g) of 10 nm. The 1 nm overlap region at the central site is highlighted with a dotted rectangle box in Fig. 1(a). With the optimal stacked sites and N_s/N_d, vertical SnSe TFETs with a shorter L_g of 7 and 5 nm and a source underlap of $UL_s = 10 - L_g$ nm are studied. The values of supply voltages (V_{dd}, equals to the bias voltage V_{ds}) of 0.74 and 0.65 V are taken
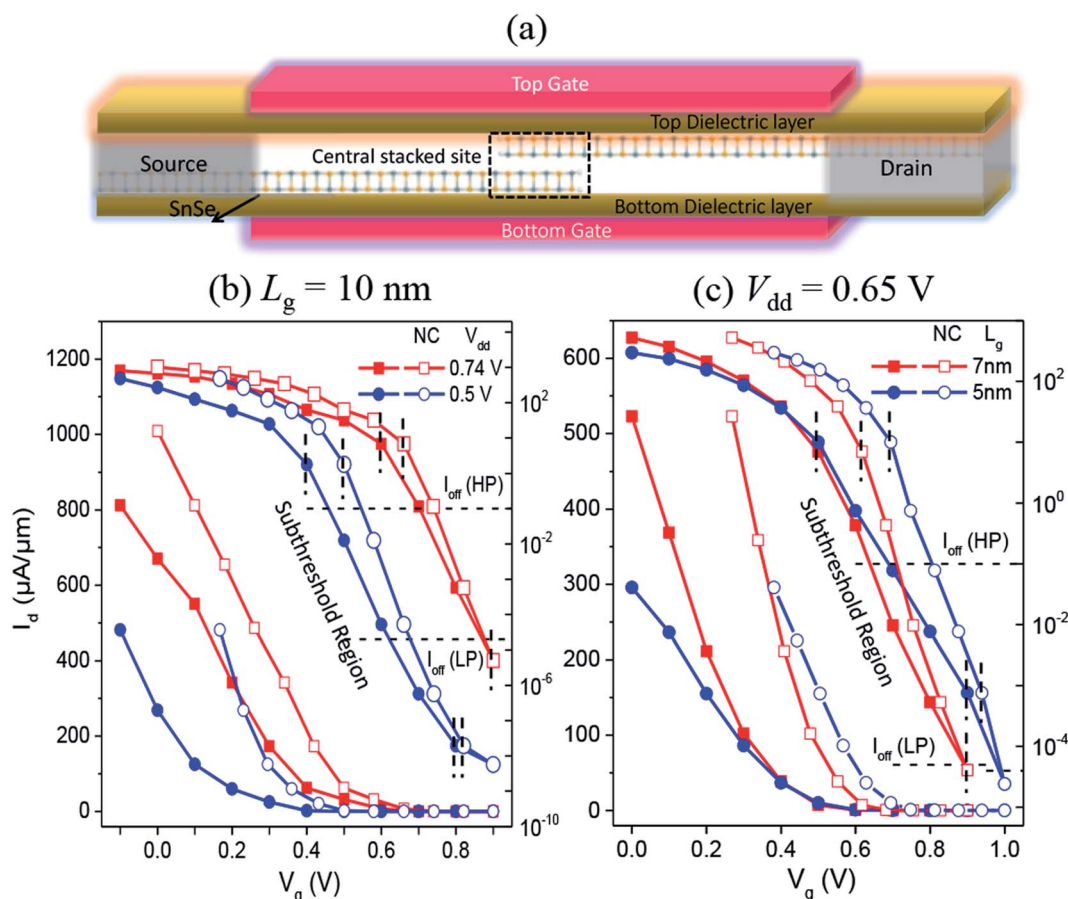

Fig. 1 (a) Device model and (b and c) transfer characteristics of the optimal sub-10 nm vertical SnSe homojunction p-TFETs and p-NCTFETs. The subthreshold region is marked with vertical black dash lines.

in regard to the International Technology Roadmap for Semiconductors (ITRS) requirements (2013 version) at similar L_g. We also scale down V_{dd} to 0.5 V for the optimal 10 nm vertical SnSe TFET.

The vertical SnSe homojunction TFETs are calculated by the DFT coupled with nonequilibrium Green's function (NEGF) using QuantumATK.[25,26] We use the same setting parameters as the DFT calculations for device simulations except for $31 \times 1 \times 151$ k-points. It's known that the GGA approximation has underestimate band gaps of intrinsic semiconductors. However, in a device model, the electrodes and channel are in a heavy doped condition, which induces a heavy screening effect to the electron–electron interaction. In the heavy doping case, the GGA approximation becomes a fine approach to the GW method for semiconductor's band gaps as discussed in a previous work.[5]

The transmission coefficient $T(E)$ is obtained by averaging $T(E,k_x)$ over 61 k_x-points, where $T(E,k_x) = T_r[G^r(E,k_x)\Gamma_s(E,k_x)G^a(E,k_x)\Gamma_d(E,k_x)]$. Then the current $I(V_{ds},V_g)$ is then derived from $T(E)$ from the Landauer–Büttiker formula:[31]

$$I(V_{ds}, V_g) = \frac{2e}{h} \int_{-\infty}^{+\infty} \left\{ T(E, V_{ds}, V_g)[f_s(E - \mu_S) - f_d(E - \mu_d)] \right\} dE$$

Here, $G^{r/a}$ is the retarded/advanced Green's function and $\Gamma_{s/d}, f_{s/d}$, and $\mu_{s/d}$ are the line width function in terms of self-energy, Fermi–Dirac distribution function, and electrochemical potential of the source/drain, respectively.

We then use a 100 nm-thick $SrBi_2Nb_2O_9$ to construct negative capacitance vertical TFETs with the SnSe stacked homojunction, where $SrBi_2Nb_2O_9$ is the best ferroelectric material among four checked ones for the ML GeSe and GeTe TFETs.[32] A negative voltage drop V_{NC} should happen across the ferroelectric layer so that a sharper subthreshold swing is expected. We calculate the V_{NC} with the Landau–Khalatnikov (L–K) theory[33] as follows:

$$V_{NC} = 2\alpha t_{Fe}Q + 4\beta t_{Fe}Q^3 + 6\gamma t_{Fe}Q^5$$

Here, t_{Fe} is the thickness and α, β, and γ the Landau coefficients of the ferroelectric layer. Q is the electrical charge on the channel calculated from Mulliken population. We set t_{Fe} to 100 nm and α, β, and γ to -3.74×10^8, -9.4×10^7, and 1.18×10^9 from a former work.[34]

3 Results and discussions

3.1 Device optimization and current

Considering the stacked sites and N_s/N_d might have some effect on currents, we first optimize I_{leak} and I_{on} of the 10 nm vertical SnSe homojunction TFET at $V_{dd} = 0.74$ V. The transfer characteristics of the vertical SnSe TFETs with stacked sites (fixed N_s/N_d of $5/5 \times 10^{13}$ cm^{-2}) are given in Fig. S1(a).† Ambipolar characters are seen for the three TFETs as N_s and N_d are the same. All I_{leak} are ~10^{-3} µA µm^{-1}, which are low enough to meet the off-state current (I_{off}) of 0.1 µA µm^{-1} of the HP devices but too high to meet I_{off} of 2×10^{-5} µA µm^{-1} of the LP devices of the ITRS requirements (2013 version). Thus, we extract I_{on} from the transfer characteristics for both p- and n-type branches and give the values in Table S2.† The central site of the stacked position is the best one for I_{on} of both the p- and n-type vertical SnSe TFETs with the values of 791 and 695 µA µm^{-1}, respectively, which meet 61% and 54% of 1287 µA µm^{-1} of the ITRS HP device.

We then pick up the vertical SnSe TFET with the central stacked site and continue to lower I_{leak} by applying an asymmetric N_s/N_d. In general, the asymmetric N_s/N_d would destroy the ambipolar characters of a TFET, and an improved I_{on} would

Table 1 Device performances of the optimal sub-10 nm vertical SnSe homojunction p-TFETs and p-NCTFETs for LP application. The ITRS requirements for LP devices and those of the planar GeSe,[5] planar BP,[35] vertical homojunction BP,[9] and vertical homojunction antimonene[35] TFETs are given for comparison. L_g: physical gate length; ULs: source underlap; V_{dd}: supply voltage; I_{off}: off-state current; I_{on}: on-state current; SS: subthreshold swing; g_m: transconductance; τ: delay time; and PDP: power dissipation

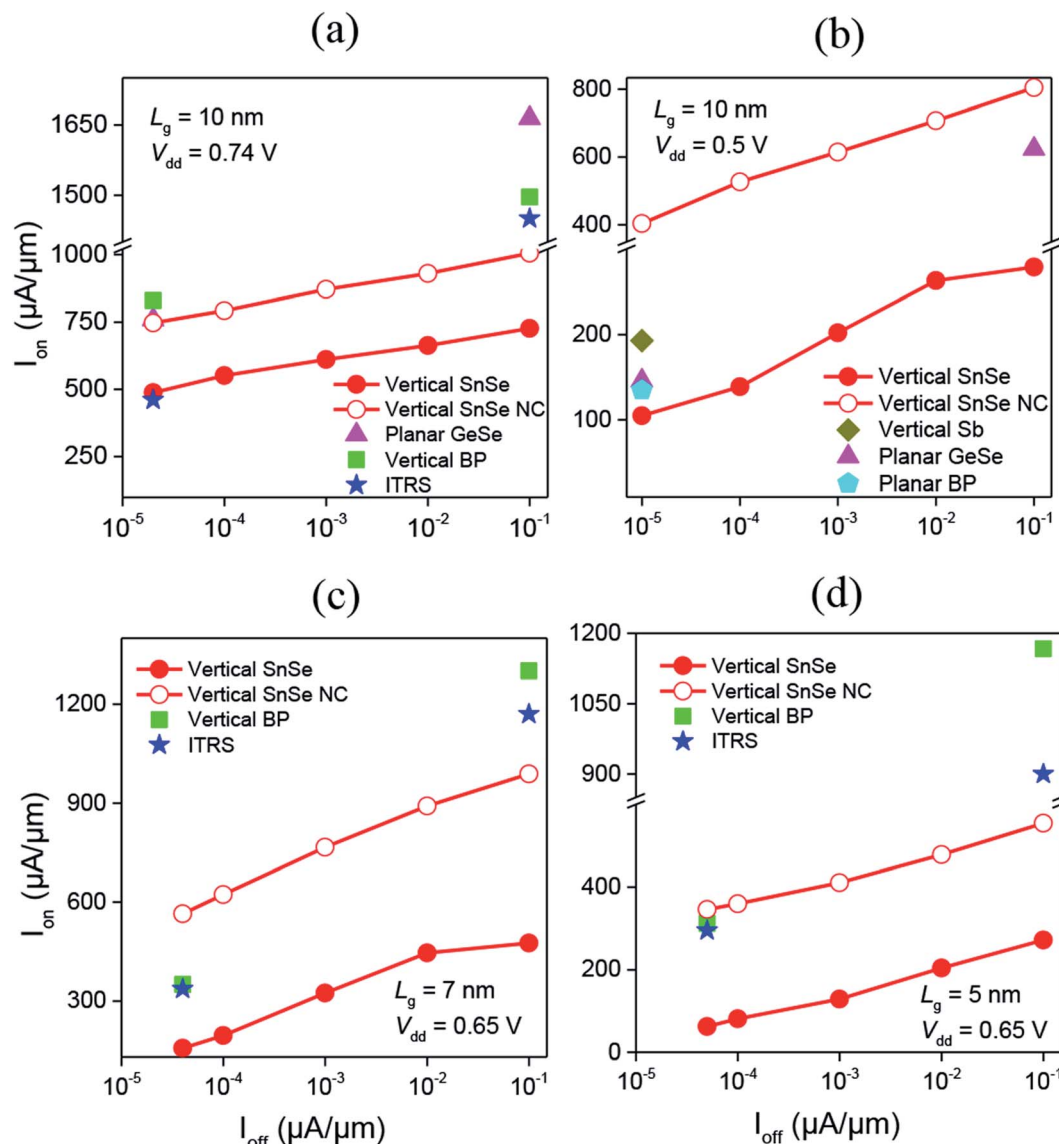|	L_g (nm)	V_{dd} (V)	UL (nm)	I_{off} (µA µm^{-1})	I_{on} (µA µm^{-1})	SS (mV dec^{-1})	g_m (mS µm^{-1})	τ (ps)	PDP (fJ µm^{-1})
Vertical SnSe	10	0.74	0	2×10^{-5}	488	48.2	1.89	0.081	0.019
Vertical SnSe NCTFET	10	0.74	0	2×10^{-5}	747	36.8	2.04	0.068	0.023
Vertical BP[9]	10	0.74	0	2×10^{-5}	830	39	4.30	0.029	0.027
Planar GeSe[5]	10	0.74	0	2×10^{-5}	759	45	3.92	0.062	0.035
ITRS 2022	10.1	0.72	—	2×10^{-5}	461	—	—	1.556	0.52
Vertical SnSe	10	0.5	0	1×10^{-5}	105	49.0	1.78	0.346	0.011
Vertical SnSe NCTFET	10	0.5	0	1×10^{-5}	404	36.7	2.77	0.133	0.017
Vertical Sb[35]	10	0.5	0	1×10^{-5}	193	22	—	—	—
Planar BP[35]	10	0.5	0	1×10^{-5}	135	33	—	—	—
Planar GeSe[5]	10	0.5	0	1×10^{-5}	146	—	—	0.19	0.014
Vertical SnSe	7	0.65	3	4×10^{-5}	157	74.5	1.56	0.278	0.018
Vertical SnSe NCTFET	7	0.65	3	4×10^{-5}	565	47.8	1.84	0.092	0.021
Vertical BP[9]	7	0.66	0	4×10^{-5}	350	63	4.23	0.063	0.018
ITRS 2026	7	0.66	—	4×10^{-5}	337	—	—	1.514	0.34
Vertical SnSe	5	0.65	5	5×10^{-5}	62	91.4	0.75	0.721	0.018
Vertical SnSe NCTFET	5	0.65	5	5×10^{-5}	346	60.1	1.14	0.154	0.021
Vertical BP[9]	5	0.64	5	5×10^{-5}	312	76	3.9	0.078	0.018
ITRS 2028	5.9	0.64	—	5×10^{-5}	295	—	—	1.493	0.28

Fig. 2 I_{on} vs. I_{off} of the optimal vertical SnSe homojunction p-TFETs and p-NCTFETs with (a) $L_g = 10$ nm and $V_{dd} = 0.74$ V, (b) $L_g = 10$ nm and $V_{dd} = 0.5$ V, (c) $L_g = 7$ nm and $V_{dd} = 0.65$ V, and (d) $L_g = 5$ nm and $V_{dd} = 0.65$ V. I_{on} of the ITRS requirements for LP and HP devices and those of the planar GeSe,[5] planar BP,[35] vertical homojunction BP,[9] and vertical homojunction antimonene[35] TFETs are given for comparison.

be acquired with a light-N_s/heavy-N_d for p-type branch and heavy-N_s/light-N_d for n-type one from previous studies.[5–7] The transfer characteristics of the vertical SnSe TFETs with N_s of 1/0.3/0.1 × 10^{13} cm^{-2} (fixed N_d of 5 × 10^{13} cm^{-2}) and N_d of 1/0.3/0.1 × 10^{13} cm^{-2} (fixed N_s of 5 × 10^{13} cm^{-2}) are drawn in Fig. S1(b) and (c),† respectively. A lower I_{leak} of 10^{-4}–10^{-7} μA μm^{-1} and an enhanced p- or n-type character are acquired as expected. I_{leak} is small enough for LP applications when either N_s or $N_d \leq 0.3 \times 10^{13}$ cm^{-2}. Benchmark of I_{on}(HP) and I_{on}(LP) against the ITRS HP/LP devices and its planar counterpart is presented in Table S3.† For HP application, the asymmetric N_s/N_d does not show a positive effect on I_{on}. Compared with its planar counterpart at the same N_s/N_d of 1/5 × 10^{13} cm^{-2}, I_{leak} decreased from ~10^{-2} to ~10^{-4} μA μm^{-1} and I_{on}(HP) from 1667 to 790 μA μm^{-1}. The descending currents come from the

interrupted carrier transport path by the structure modification of vertical stacking. For LP application, the lightest N_s or N_d is the best. In the following, we will focus on the device performances of the enhanced p-type region of the optimal vertical SnSe homojunction TFETs with central stacked sites and N_s/N_d = 0.1/5 × 10^{13} cm^{-2} for LP applications.

The transfer characteristics of the sub-10 nm optimal vertical SnSe homojunction p-TFETs are given in Fig. 1(b and c), and the key figures of merit for LP applications are presented in Table 1. As L_g decreases to 7/5 nm, I_{leak} is also low enough to meet I_{off} of 4/5 × 10^{-5} μA μm^{-1} of the ITRS LP devices. The ITRS targets for LP devices and the device performances of the planar GeSe,[5] planar BP,[35] vertical homojunction BP,[9] and vertical homojunction antimonene[35] TFETs are given for comparison in Table 1. We provide I_{on} as a function of I_{off} of the SnSe homojunction
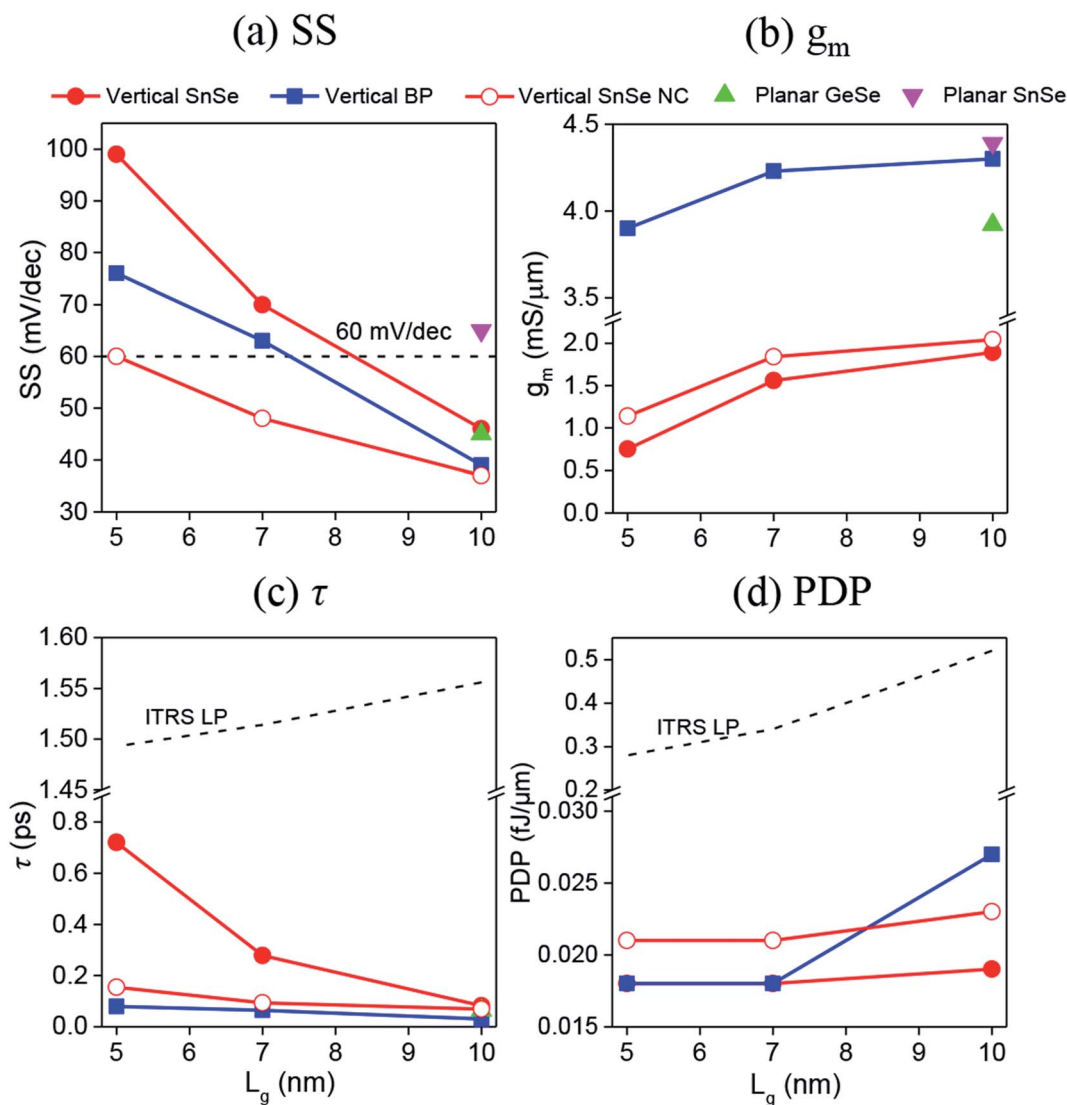
Fig. 3 (a) SS, (b) g_m, (c) τ, and (d) PDP as a function of L_g of the optimal sub-10 nm vertical SnSe homojunction p-TFETs and p-NCTFETs ($V_{dd} = 0.64-0.74$ V) compared with those of the ITRS requirements for LP devices and those of the planar GeSe[5] and vertical homojunction BP.[9]

p-TFETs ($L_g = 5-10$ nm, $V_{dd} = 0.5-0.74$ V) and I_{on} of the devices mentioned above in Fig. 2(a–d). The optimal I_{on}(LP) are 488, 146, and 62 µA µm^{-1} for the vertical SnSe p-TFET at $L_g = 10$, 7, and 5 nm, respectively, which surpass or meet 43% and 21% of 461, 337, and 195 µA µm^{-1} of the 2022, 2026, and 2028 targets of the ITRS LP devices (2013 version) at similar L_g, respectively. As seen in Fig. 2, when I_{off} increases by ∼4 orders of magnitude from ∼10^{-5} to 10^{-1} µA µm^{-1}, I_{on} increases slowly by 1.5–4.1 times, and the increment is more notable for the TFET with a shorter L_g or at a lower V_{dd}. Though I_{on} of the vertical SnSe p-TFET show no goodness when compared to other sub-10 nm TFETs, it's worthy to note that I_{on} of 105 µA µm^{-1} of the 10 nm vertical SnSe p-TFET is comparable with those of 135–193 µA µm^{-1} of the vertical antimonene TFET and the planar phosphorene and GeSe TFETs at $V_{dd} = 0.5$ V.[5,35]

3.2 Gate control ability and dynamic performance metrics

The gate control abilities are described by the subthreshold swing $\left(\mathrm{SS} = \dfrac{\partial V_g}{\partial \lg I_D}\right)$ and transconductance $\left(g_m = \dfrac{\mathrm{d}I_D}{\mathrm{d}V_g}\right)$ in the subthreshold and superthreshold regions, respectively. A smaller SS (or a larger g_m) stands for a stronger gate control ability. We give SS (in the subthreshold region as marked in Fig. 1) and g_m of the sub-10 nm optimal vertical SnSe homojunction p-TFET compared with those of the vertical BP and planar GeSe and SnSe TFETs[5,9] in Fig. 3(a and b). The subthreshold regions cover five to eight decades of currents for all the vertical SnSe p-TFETs. Both an increasing SS (48.2 to 91.4 mV dec^{-1}) and decreasing g_m (1.89 to 0.75 mS µm^{-1}) with the decreasing L_g are seen for the vertical SnSe p-TFETs, which indicates the descending gate control ability with the decreasing L_g in both subthreshold and superthreshold regions. The slightly larger SS and much smaller g_m of the vertical SnSe
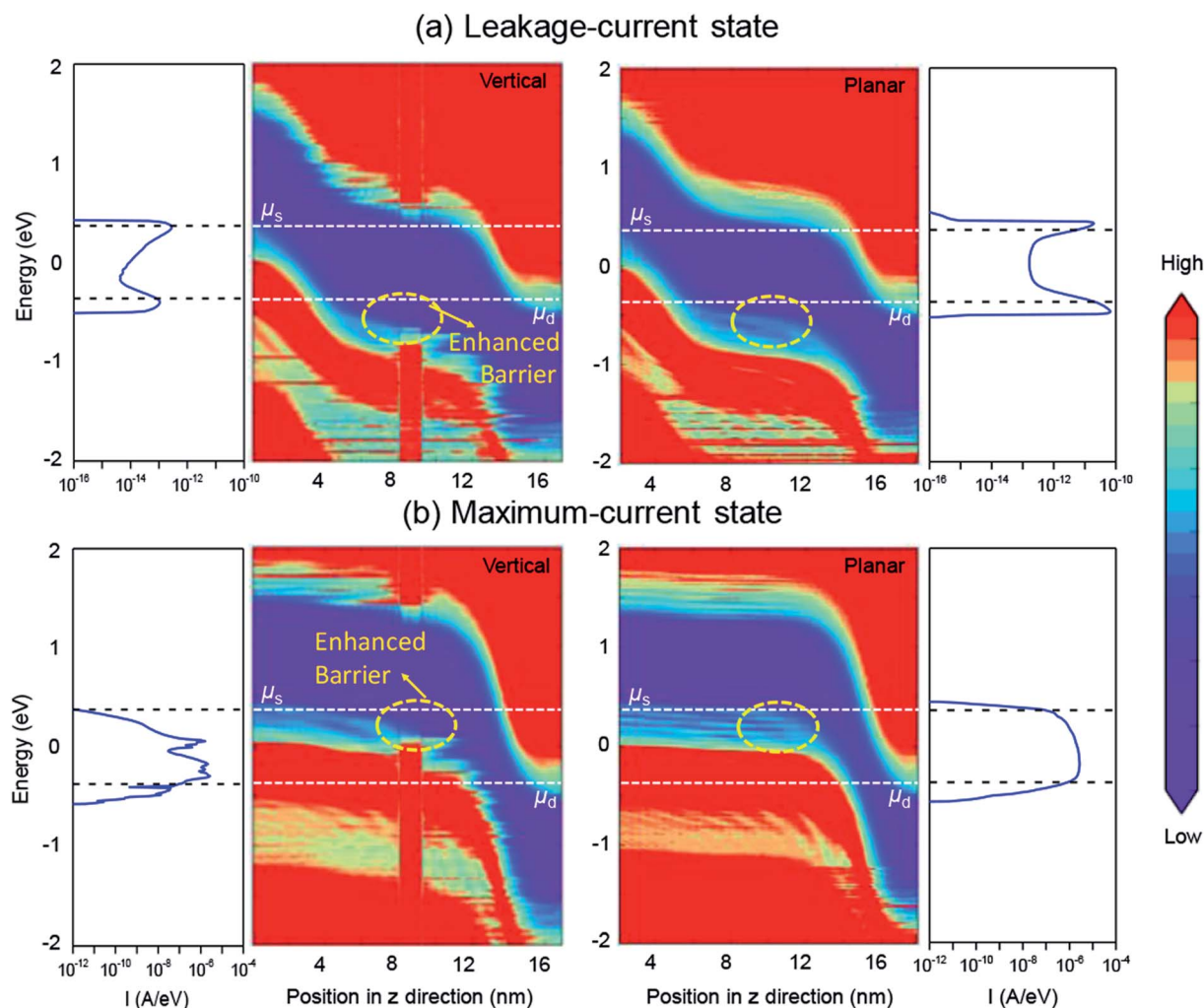
Fig. 4 Local device density of states (LDDOS) and spectral currents of the optimal vertical SnSe homojunction p-TFETs with $L_g = 10$ nm at $V_{dd} = 0.74$ V compared with those of the planar counterpart for the (a) leakage-current state and (b) maximum-current state.

p-TFETs compared with those of the vertical BP and planar GeSe TFETs[5,9] at the same L_g indicate a slightly weaker gate control in the subthreshold region and a much weaker gate control in the superthreshold regions, respectively. Whereas, in regard to its SnSe planar counterpart,[5] much enhanced and descended gate controls are found in the subthreshold and superthreshold regions, respectively.

The average SS over four decades of current ($SS_{ave\_4\ dec}$) and the drain current at SS = 60 mV dec^{-1} (I_{60}) are regarded as two metrics for fast low-power devices. Basically, $SS_{ave\_4\ dec}$ below 60 mV dec^{-1} and I_{60} above 1 μA μm^{-1} are asked for a fast low-power device. We present the minimum SS (SS_{min}), $SS_{ave\_4\ dec}$, and I_{60} of the vertical SnSe p-TFETs in Table S4.† The sharp SS_{min} is harder to maintain over decades of current in the vertical SnSe p-TFETs with shorter L_g. Sub-thermionic SS_{min} and $SS_{ave\_4\ dec}$ and high I_{60} are only obtained for the 10 nm vertical SnSe p-TFET, *i.e.*, SS_{min} of 42.0–43.4 mV dec^{-1}, $SS_{ave\_4\ dec}$ of 44.2–45.8 mV dec^{-1}, and I_{60} of 5–7 μA μm^{-1} at $V_{dd} = 0.5$–0.74 V. For the 7 and 5 nm vertical SnSe p-TFETs, SS_{min} are 60.7 and

66.7 mV dec^{-1} and $SS_{ave\_4\ dec}$ are 71.2 and 90.1 mV dec^{-1}, respectively.

The device dynamic performance metrics are represented by the intrinsic delay time $\left(\tau = \dfrac{Q_{on} - Q_{off}}{W \times I_{on}} \right)$ and the power delay product $\left(PDP = \dfrac{(Q_{on} - Q_{off}) \times V_{dd}}{W} \right)$, which define the switching speed and energy consumption of a transistor, respectively. Here, $Q_{on/off}$ is the on-/off-state overall charge of the channel and W the channel width. We benchmark τ and PDP of the vertical SnSe p-TFETs against the ITRS LP devices and the planar GeSe and vertical BP TFETs[5,9] in Fig. 3(c and d). τ of the vertical SnSe p-TFET increases rapidly from 0.156 to 0.721 ps with the decreasing L_g from 10 to 5 nm, indicating an obvious decaying of the device switching speed with the decreasing L_g. τ of the vertical SnSe p-TFET is half to one-tenth of 1.493–1.556 ps of the ITRS LP devices, but much larger than those of the planar GeSe and vertical BP TFETs at the same L_g. The vertical SnSe p-TFET shows a generally better behavior on energy consumption

at a shorter L_g as a decreasing trend of PDP is seen. PDP of 0.018–0.035 fJ μm^{-1} of the vertical SnSe p-TFET is more than one order of magnitude below the ITRS LP devices (0.28–0.52 fJ μm^{-1}) and nearly equal to those of the planar GeSe and vertical BP TFETs[5,9] at the same L_g.

3.3 Negative capacitance

The vertically stacked homojunction has a prominent effect of lowering I_{leak} of its planar counterpart, but unfortunately, I_{on} descends as well. We then import negative capacitance to make the SS sharper and therefore to improve I_{on}. The transfer characteristics of the vertical SnSe p-NCTFETs with a 100 nm-thick ferroelectric layer of $SrBi_2Nb_2O_9$ are given in Fig. 1(b and c). A remarkable enhanced of I_{on} by 53–458% is obtained as given in Table 1 and Fig. 2. I_{on} of 565 and 346 μA μm^{-1} of the vertical SnSe NCTFETs surpass the 2026 and 2028 targets of 337 and 295 μA μm^{-1} of the ITRS LP device at L_g = 7 and 5 nm, respectively. At a lower V_{dd} = 0.5 V, I_{on} of 404 μA μm^{-1} of the 10 nm vertical SnSe NCTFET is 2–3 times the vertical anti-monene TFET and the planar phosphorene and GeSe TFETs.[5,35] The SS and g_m of the vertical SnSe NCTFETs are given in Table 1 and Fig. 3(a and b). SS decrease to 36.7–60.1 mV dec^{-1} and g_m increase to 1.14–2.77 mS μm^{-1}, implying an enhanced gate control of the NCTFET counterpart. τ decrease to 0.068–0.154 ps and PDP increase slightly to 0.017–0.023 fJ μm^{-1} as given in Table 1 and Fig. 3(c and d).

3.4 LDDOS, spectral current, and discussion

The local device density of states (LDDOS) together with spectral currents of the vertical SnSe p-TFET at V_g = 1.0 V (leakage current) and 0.0 V (maximum current) compared with its planar counterpart are presented in Fig. 4. An obvious enhanced barrier can be seen from the LDDOS of the vertical SnSe p-TFET for both the leakage-current and maximum-current states, which results in a sound decreasing of spectral currents. As a result, this vertically stacked modification of the SnSe TFET lower the leakage current of its planar counterpart by 2–3 orders of magnetite, but an unwanted descendant of I_{on} by around a half is accompanied.

In a word, the structural modification of vertical stacking is a certainly effective solution to lower I_{leak} of a TFET, and we have succeeded in tuning the SnSe TFET from HP device to LP device in this work and extending the BP TFET to LP application.[9] And to import a ferroelectric layer is a remarkable method to improve I_{on}. Noteworthily, this vertically stacked modification and negative capacitance introduction of a TFET structure is a prototype method, and could easily apply to other 2D planar TFETs, like the Bi and GeTe TFETs,[8,32] which possess both high I_{leak} and I_{on} simultaneously.

For the realization of 2D FETs in labs, sub-5 nm traditional FETs are reported based on the channel material of ML MoS_2,[36] bilayer MoS_2,[37] and bilayer $MoTe_2$.[38] For 2D BP traditional FETs, the shortest experiment reported gate length is 20 nm.[39] As for 2D TFETs, the progress in experiment is much behind the traditional FETs. To the best of our knowledge, there're no reports of 2D TFETs in the nanometer scale. Recently, the

vertical homojunction TFETs based on multilayer BP have been realized in the micrometer scale in labs.[40,41] As an analog of BP, 2D SnSe is widely studied in recent years[42–44] but rarely reported as FET despite its excellent electronic properties like BP and good air-stability over BP. Our theoretical predicted good device performances of the sub-10 nm vertical SnSe homojunction TFET for a fast LP application would certainly encourage the corresponding experimental studies.

4 Conclusions

To summarize, we investigate the device performances of the sub-10 nm vertical SnSe homojunction TFETs with *ab initio* quantum transport calculations. The vertically stacked device configuration of the SnSe TFET is beneficial for a fast low-power device in regard to the planar configuration because the broken connected top and bottom layers lead to an enhanced transport barrier. $SS_{ave\_4\ dec}$ of 44.2–45.8 mV dec^{-1} and I_{60} of 5–7 μA μm^{-1} are obtained for the optimal vertical SnSe homojunction TFET with L_g = 10 nm at V_{dd} = 0.5–0.74 V. In terms of I_{on}, intrinsic τ, and PDP, the vertical SnSe TFETs and NCTFETs outperform the 2022 and 2028 targets of the ITRS low-power device (2013 version), respectively. The impressive performance of the vertical SnSe TFETs would accelerate future TFET manufacturing.

Conflicts of interest

There are no conflicts to declare.

Acknowledgements

References

1 G. Fiori, F. Bonaccorso, G. Iannaccone, T. Palacios, D. Neumaier, A. Seabaugh, S. K. Banerjee and L. Colombo, *Nat. Nanotechnol.*, 2014, **9**, 768–779.

2 M. Chhowalla, D. Jena and H. Zhang, *Nat. Rev. Mater.*, 2016, **1**, 16052.

3 H. Lu and A. Seabaugh, *IEEE J. Electron Devices Soc.*, 2014, **2**, 44–49.

4 Y. Lv, W. Qin, C. Wang, L. Liao and X. Liu, *Adv. Electron. Mater.*, 2019, **5**, 1800569.

5 H. Li, P. Xu and J. Lu, *Nanoscale*, 2019, **11**, 23392–23401.

6 H. Li, B. Shi, Y. Pan, J. Li, L. Xu, X. Zhang, F. Pan and J. Lu, *Nanotechnol*, 2018, **29**, 485202.

7 H. Li, J. Tie, J. Li, M. Ye, H. Zhang, X. Zhang, Y. Pan, Y. Wang, R. Quhe, F. Pan and J. Lu, *Nano Res.*, 2018, **11**, 2658–2668.

8 H. Li, P. Xu, L. Xu, Z. Zhang and J. Lu, *Semicond. Sci. Technol.*, 2019, **34**, 085006.

9 H. Li and J. Lu, *Appl. Surf. Sci.*, 2019, **465**, 895–901.

10 H. Du, X. Lin, Z. Xu and D. Chu, *J. Mater. Chem. C*, 2015, **3**, 8760–8775.

11 A. Carvalho, M. Wang, X. Zhu, A. S. Rodin, H. Su and A. H. Castro Neto, *Nat. Rev. Mater.*, 2016, **1**, 16061.

12 M. Akhtar, G. Anderson, R. Zhao, A. Alruqi, J. E. Mroczkowska, G. Sumanasekera and J. B. Jasinski, *npj 2D Mater. Appl.*, 2017, **1**, 5.

13 W. C. Tan, L. Wang, X. Feng, L. Chen, L. Huang, X. Huang and K.-W. Ang, *Adv. Electron. Mater.*, 2019, **5**, 1800666.

14 J.-S. Kim, Y. Liu, W. Zhu, S. Kim, D. Wu, L. Tao, A. Dodabalapur, K. Lai and D. Akinwande, *Sci. Rep.*, 2015, **5**, 8989.

15 D. He, Y. Wang, Y. Huang, Y. Shi, X. Wang and X. Duan, *Nano Lett.*, 2019, **19**, 331–337.

16 B. Wan, B. Yang, Y. Wang, J. Zhang, Z. Zeng, Z. Liu and W. Wang, *Nanotechnol*, 2015, **26**, 435702.

17 M.-H. Jeong, D.-H. Kwak, H.-S. Ra, A. Y. Lee and J.-S. Lee, *ACS Appl. Mater. Interfaces*, 2018, **10**, 19069–19075.

18 J. Jiang, C. P. Y. Wong, J. Zou, S. Li, Q. Wang, J. Chen, D. Qi, H. Wang, G. Eda, D. H. C. Chua, Y. Shi, W. Zhang and A. T. S. Wee, *2D Mater.*, 2017, **4**, 021026.

19 Y. Huang, L. Li, Y.-H. Lin and C.-W. Nan, *J. Phys. Chem. C*, 2017, **121**, 17530–17537.

20 L. Li, Z. Chen, Y. Hu, X. Wang, T. Zhang, W. Chen and Q. Wang, *J. Am. Chem. Soc.*, 2013, **135**, 1213–1216.

21 L. Xu, M. Yang, S. J. Wang and Y. P. Feng, *Phys. Rev. B*, 2017, **95**, 235434.

22 Y. Guo, S. Zhou, Y. Bai and J. Zhao, *ACS Appl. Mater. Interfaces*, 2017, **9**, 12013–12020.

23 L.-B. Shi, M. Yang, S. Cao, Q. You, Y.-Y. Niu and Y.-Z. Wang, *Appl. Surf. Sci.*, 2019, **492**, 435–448.

24 L. C. Gomes, A. Carvalho and A. H. C. Neto, *Phys. Rev. B*, 2016, **94**, 054103.

25 *QuantumATK, version P-2019.03*, http://www.synopsys.com/silicon/quantumatk.html.

26 S. Smidstrup, T. Markussen, P. Vancraeyveld, J. Wellendorff and K. Stokbro, *J. Phys.: Condens. Matter*, 2020, **32**, 015901.

27 J. P. Perdew, K. Burke and M. Ernzerhof, *Phys. Rev. Lett.*, 1996, **78**, 3865–3868.

28 S. Grimme, *J. Comput. Chem.*, 2006, **27**, 1787–1799.

29 H. J. Monkhorst, *Phys. Rev. B: Solid State*, 1976, **13**, 5188–5192.

30 Y. C. Huang, X. Chen, C. Wang, L. Peng, Q. Qian and S. F. Wang, *Nanoscale*, 2017, **9**, 8616–8622.

31 S. Datta, *Electronic Transport in Mesoscopic Systems*, Cambridge University Press, Cambridge, England, 1995.

32 P. Xu, J. Liang, H. Li, F. Liu, J. Tie, Z. Jiao, J. Luo and J. Lu, *RSC Adv.*, 2020, **10**, 16071.

33 A. Starkov and I. Starkov, *Ferroelectrics*, 2014, **461**, 50–60.

34 F. Liu, Y. Zhou, Y. Wang, X. Liu, J. Wang and H. Guo, *npj Quantum Mater.*, 2016, **1**, 16004.

35 J. Chang, *Nanoscale*, 2018, **10**, 13652–13660.

36 L. Xie, M. Liao, S. Wang, H. Yu, L. Du, J. Tang, J. Zhao, J. Zhang, P. Chen and X. Lu, *Adv. Mater.*, 2017, **29**, 1702522.

37 S. B. Desai, S. R. Madhvapathy, A. B. Sachid, J. P. Llinas, Q. Wang, G. H. Ahn, G. Pitner, M. J. Kim, J. Bokor and C. Hu, *Science*, 2016, **354**, 99–102.

38 Q. Zhang, X.-F. Wang, S.-H. Shen, Q. Lu, X. Liu, H. Li, J. Zheng, C.-P. Yu, X. Zhong, L. Gu, T.-L. Ren and L. Jiao, *Nat. Electron.*, 2019, **2**, 164–170.

39 J. Miao, S. Zhang, L. Cai, M. Scherr and C. Wang, *ACS Nano*, 2015, **9**, 9236–9243.

40 S. Kim, G. Myeong, W. Shin, H. Lim, B. Kim, T. Jin, S. Chang, K. Watanabe, T. Taniguchi and S. Cho, *Nat. Nanotechnol.*, 2020, **15**, 203–206.

41 P. Wu and J. Appenzeller, *IEEE Electron Device Lett.*, 2019, **40**, 981–984.

42 X. Zhou, Q. Zhang, L. Gan, H. Li, J. Xiong and T. Zhai, *Adv. Sci.*, 2016, **3**, 1600177.

43 W. Shi, M. Gao, J. Wei, J. Gao, C. Fan, E. Ashalley, H. Li and Z. Wang, *Adv. Sci.*, 2018, **5**, 1700602.

44 W. Huang, C. Li, L. Gao, Y. Zhang, Y. Wang, Z. N. Huang, T. Chen, L. Hu and H. Zhang, *J. Mater. Chem. C*, 2020, **8**, 1172–1197.